

# A Data-Driven Approach to Geometric Modeling of Systems with Low-Bandwidth Actuator Dynamics

Siming Deng<sup>1,2,\*</sup>, Junning Liu<sup>2</sup>, Bibekananda Datta<sup>2</sup>, Aishwarya Pantula<sup>3</sup>, David H. Gracias<sup>3</sup>,  
Thao D. Nguyen<sup>2</sup>, Brian A. Bittner<sup>4,†</sup>, Noah J. Cowan<sup>1,2,†,\*</sup>

**Abstract**—It is challenging to perform identification on soft robots due to their underactuated, high dimensional dynamics. In this work, we present a data-driven modeling framework, based on geometric mechanics (also known as gauge theory), that can be applied to systems with low-bandwidth actuation of the shape space. By exploiting temporal asymmetries in actuator dynamics, our approach enables the design of robots that can be driven by a single control input. We present a method for constructing a series connected model comprising actuator and locomotor dynamics based on data points from stochastically perturbed, repeated behaviors around the observed limit cycle. We demonstrate our methods on a real world example of a soft crawler made by stimuli-responsive hydrogels that locomotes on merely one cycling control signal by utilizing its geometric and temporal asymmetry. For systems with first-order, low-pass actuator dynamics, such as swelling-driven actuators used in hydrogel crawlers, we show that first order Taylor approximations can well capture the dynamics of the system shape as well as its movements. Finally, we propose an approach of numerically optimizing control signals by iteratively refining models and optimizing the input waveform.

## I. INTRODUCTION

Many traditional robots rely predominantly on rigid, fully actuated mechanisms. While these robots maintain superior force and precision compare to natural organisms, these rigid machines usually struggle in tasks that involve safe interactions with humans, handling deformable objects, and operations in unstructured environments [1]. Designs from nature have inspired the development of compliant mechanisms in robotics, enabling new capabilities [2]–[6]. The emergence of such soft components in modern robotic platforms has provided new avenues to improved adaptability, safety, cost, and energy efficiency. On the other hand, the compliant nature of these soft components greatly increases the internal degrees of freedom as well as the degree of underactuation. Specifically, soft actuators such as pressure-powered [2], [7], [8] or stimuli-driven devices [9]–[12] usually exhibit nonlinear or coupled (i.e. multiple body segments reacting

This material is based upon work supported by the National Science Foundation under grants no. #1830893, EFRI C3 SoRo: Programming Thermobiochemomechanical (TBCM) Multiplex Robot Gels

<sup>1</sup>Laboratory for Computational Sensing and Robotics, Johns Hopkins University, Baltimore MD 21218 USA.

<sup>2</sup>Department of Mechanical Engineering, Johns Hopkins University, Baltimore MD 21218 USA.

<sup>3</sup>Department of Chemical and Biomolecular Engineering, Johns Hopkins University, Baltimore MD 21218 USA.

<sup>4</sup>Johns Hopkins University Applied Physics Lab, Laurel, MD, 97331 USA.

<sup>†</sup>Co-supervised equally.

\*To whom correspondence should be addressed: <sdeng10, ncowan>@jhu.edu

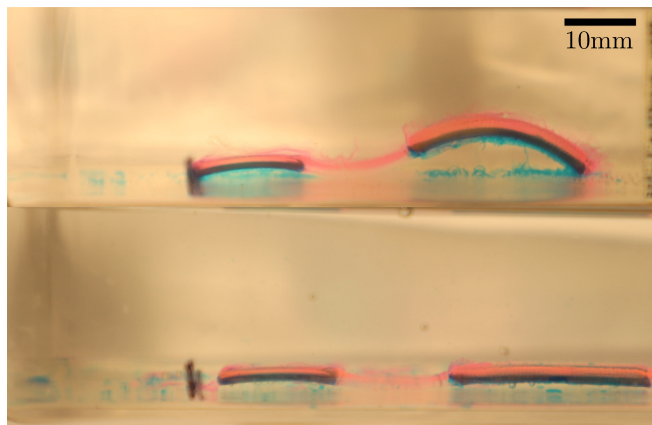


Fig. 1. Experimental screenshots of thermal cycling of two-segment robots with a flexible linker at the end of (top) cooling half-cycle (b) heating half-cycle. One thermal cycle comprises of a heating half-cycle and a cooling half-cycle. Robot displaces 4.4% at the end of cycle.

to the same excitation signal in different ways) dynamics, such as change in shape or frictional behavior in response to applied temperature, light, and electromagnetic field, in their actuation. It is often considered a luxury to obtain precise control of the system shape of a soft actuator. One possibility is to leverage low-bandwidth, passive responses to stimuli as a means of locomotion, taking advantage of differences in temporal dynamics between subsystems or components. In this work, we investigate such passive responses within a systematic framework for control of soft systems, focusing on systems with low-bandwidth shape changes in response to a single actuator input. Modeling actuator dynamics and its effects on the system can streamline engineering efforts to design and control soft robots, maximizing their capabilities with less exploratory or exhaustive experimentation. For dissipative systems with high bandwidth control in shape, previous work has been done creating a mathematical framework to model, plan, and optimize robot behaviors [13], [14], and the same framework has been instrumental in understanding cyclic animal locomotion [15], [16]. The core premise underlying this work is that complex locomotor mechanics can be rewritten in a kinematic form, owing to the assumption that Rayleigh dissipation dominates [17]. Here, the body velocity of the system is a shape defined linear mapping of shape velocity. The challenges of precise fabrication and sensing make it infeasible to build the model from first principles for any practical systems. Bittner et

al. [18] presented a data-driven approach to this problem: instead of a global model, their method constructs a local model in the neighborhood of the observed limit cycle, using data points from stochastically perturbed, repeated behaviors. More recent work [19] extended this data-driven approach to shape-underactuated systems, which only have high bandwidth control available to a subset of the shape space. The ability to build local models provides the opportunity to sample candidate gaits offline for sample efficient hardware-in-the-loop optimization.

Here, we extend data-driven geometric mechanics modeling methods to platforms with *low-bandwidth control* distributed across the shape space, motivated by our prior work with a realized soft robot made of hydrogel [20], see Fig. I. In this prior work, we conceptualized and built a thermo-responsive hydrogel crawler. Although stimuli-responsive shape changes for hydrogels are ubiquitous in literature [21]–[23], the design of our robot exploited the swelling and shrinking induced bending mechanism, morphological asymmetry, and asymmetry in friction force in response to the change in surrounding temperature to achieve the locomotion. In this crawler, there are three distinct segments: a suspended linker segment connects two end bilayer segments comprising active poly(*N*-isopropylacrylamide) (pNIPAM) and passive polyacrylamide (pAAM) layers with different morphologies. Asymmetry in friction forces, caused by morphological asymmetry, between the two bilayer segments at low and high temperature allowed the robot to change its anchor during a temperature cycle to move unidirectionally. Additionally, we also hypothesize that the relative swelling speeds of these bilayers create such asymmetric ground interactions (primarily friction forces) that can be exploited for locomotion. Utilizing the asymmetric response time among segments, this robot is able to locomote with a single cyclic input—temperature cycles. Along side the fabrication of this physical crawler, we also developed an Finite Element Analysis (FEA) model in [20] to simulate the response and investigate the deformation mechanisms. In this paper, the hydrogel crawler data is generated from the FEA model.

Our core contribution, presented in Section III, is an extension of the current data-driven modeling techniques of drag dominated systems to a more challenging class of underactuated systems, where the entire shape is subject to a low-bandwidth control input (where prior work [19] required at least one element to be accessed by high bandwidth control). In IV, we demonstrate our methods on a well known, analytically tractable system, that has been modified so to include low-bandwidth actuation of its shape parameters. Finally, in Section V we test our methods on a high-dimensional, finite element model of our previously published hydrogel robot [20]. In both examples, we show how the actuator dynamics can be simultaneously modeled with the body movements, enabling a data-driven modeling architecture for a broader class of soft or underactuated systems. Further, we use these examples to numerically optimize a parameterized input signal for certain objectives using an iterative parameter

optimization and model refinement approach.

## II. BACKGROUND

### A. Geometric locomotion model

Geometric mechanics [17], [24], [25] provides a framework for locomotion based on exploiting symmetry. A core result from this field is the reduced Lagrangian or reconstruction equation, which makes the distinction between the internal configuration (shape) of a locomotion system and its position and orientation (group) in a spatially fixed reference frame. Central to this framework is the idea of group invariance of the dynamics [26]: a shape change that moves the system in a certain way—in the system body frame—will do the same at any position and orientation in the environment, invariant to the absolute position and orientation.

Here, we consider a subclass of such group-invariant systems that are dominated by Rayleigh dissipation as caused by many types of isotropic friction [27]; in such dissipation-dominated systems, the equations of motion can be kinematically reduced such that the body velocity is expressed as a shape-defined linear mapping of shape velocity. In this case, the kinematic equation can be written as

$$(g^{-1}\dot{g})^\vee = \xi = -\mathbf{A}(r)\dot{r}, \quad (1)$$

where  $\xi$  the group velocity in its body frame<sup>1</sup>,  $r$  denotes the system shape, and  $\mathbf{A}(r)$  is called the *local connection*. Here the matrix  $\mathbf{A}(r)$  is a function of shape  $r$  and acts analogously to a Jacobian in which it relates the system’s shape velocities to body velocities. A spatial trajectory of the system body frame can be calculated by integrating (1) with respect to a fixed reference frame.

For systems within the scope of (1), the local connection can be analytically derived from a set of Pfaffian constraints on the system’s shape and body velocities. A global model can be empirically estimated by exhaustively sampling the system shape space and its tangent bundle (the collection of shape velocities available at each point in the shape space) [28]. However, such global models are often difficult to obtain for animals or underactuated systems because of the challenges in sampling this space with sufficient density.

### B. Data-driven modeling

Bittner et al. [18] developed a data-driven approaches to geometric modeling and optimization, an approach that was later extended [19] to be applied to systems with high bandwidth control in only a subset of the shape variables. This approach allows a local estimation of a connection in the neighborhood of a limit cycle with far fewer samples than required to train a global model, making it practical for *in-situ* system identification, especially for systems with high dimensional shape spaces.

In this approach, data (including the system shape and position in the form of a regularly sampled time series) are fit

<sup>1</sup>Here  $(\cdot)^\vee$  is an isomorphism that maps velocities from the lie algebra form to a vector form, and its inverse is denoted as  $(\cdot)^\wedge$ . In a SE(2) case,  $(\cdot)^\vee : se(2) \rightarrow \mathbb{R}^3$ , and  $(\cdot)^\wedge : \mathbb{R}^3 \rightarrow se(2)$

to an oscillator such that each data point is assigned a phase value [29]. A zero-phase-lag butterworth smoothing filter is applied before finite differencing to obtain time derivatives of both shape and position. Then, a local Taylor approximation of the connection can be computed via linear regression across data points within phase windows. A Fourier series is then fit to these local regression coefficients to build a model that is supported at any queried phase.

We detail the process by which we estimate a linearized model within each phase window. Data-driven floquet analysis techniques extract information from the observed oscillator data and assign each sample point an estimated phase [30]. The observed shape samples are then phase-averaged and fitted to a Fourier series to obtain a limit cycle, denoted as  $\theta_r(\cdot)$ . The perturbed trajectory, relative to the limit cycle, is denoted as  $\delta_r := r - \theta_r$ . The first order Taylor approximation of the local connection in each local phase window can be constructed as

$$\mathbf{A}_k(r) \approx \mathbf{A}_k(\theta_r) + \delta_r^T \frac{\partial \mathbf{A}_k}{\partial r}, \quad (2)$$

where  $\mathbf{A}_k(r)$  is the  $k^{\text{th}}$  row of the local connection, which is a vector of the same dimension as shape perturbation  $\delta_r$ .

All samples are grouped into neighborhoods by their estimated phase values, and a local model is fitted in each phase window. In the  $m^{\text{th}}$  phase window, the averaged shape is assumed to be a constant  $\theta_r^m$ . The first order Taylor approximation of the local connection matrix  $\mathbf{A}(r)$  in this phase window can be fitted by solving the following Generalized Linear Model (GLM):

$$\xi_k^{(n)} \sim \mathbf{C}_k + \mathbf{B}_k \delta_r^{(n)} + \mathbf{A}_k(\theta_r) \dot{\delta}_r^{(n)} + \frac{\partial \mathbf{A}_k}{\partial r} \delta_r^{(n)} \dot{\delta}_r^{(n)}. \quad (3)$$

Here,  $\xi_k^{(n)}$  corresponds to the  $k^{\text{th}}$  coordinate of the  $n^{\text{th}}$  sampled body velocity  $\xi^{(n)}$ , and  $\delta_r^{(n)} := r^{(n)} - \theta_r^m$ ,  $\dot{\delta}_r^{(n)} := \dot{r}^{(n)} - \dot{\theta}_r^m$  are the shape and shape velocity perturbation samples defined in the local region indexed by  $m$ . Regressor  $\mathbf{C}_k := \mathbf{A}_k(\theta_r) \theta_r$  describes the average behavior in the neighborhood of  $\theta_r^m$ .  $\mathbf{B}_k := \dot{\theta}_r^T \frac{\partial \mathbf{A}_k}{\partial r}$  and  $\mathbf{A}_k$  are the terms that respectively relate the effects of shape and shape velocity offsets from the limit cycle.  $\frac{\partial \mathbf{A}_k}{\partial r}$  is the cross term that incorporates the interaction between  $\delta_r$  and  $\dot{\delta}_r$ . Note that this is a local estimate in the  $m^{\text{th}}$  phase window. This local approximation is repeated for all separate groups of data points, after which a Fourier series model is used to guarantee a smooth transition among the fitted matrices.

### III. METHODS

#### A. Low bandwidth shape control

In this paper, we consider systems whose locomotion can be characterized by (1) while only having access to low bandwidth control over  $r$ . In particular, we assumed the dynamics on  $r$  to take the general form of

$$\dot{r} = f(r, u), \quad (4)$$

where the system shape velocity  $\dot{r}$  is a function of its shape  $r$  and an input  $u$ .

First, we extracted a phase-averaged gait cycle  $(\theta_r, \theta_u)$  from the general input [29]. Denoting the perturbation from phase-averaged shape and control as  $\delta_r := r - \theta_r$ ,  $\delta_u := u - \theta_u$ , the local first order Taylor approximation of the actuation dynamics can be written in the following form:

$$f(r, u) \approx f(\theta_r, \theta_u) + \frac{\partial f}{\partial r}(\theta_r, \theta_u) \delta_r + \frac{\partial f}{\partial u}(\theta_r, \theta_u) \delta_u \quad (5)$$

We then fit the data to the above first order approximation by solving the following Generalized Linear Model,

$$\dot{\delta}_r^{(n)} \sim \mathbf{D} + \mathbf{E}_r \delta_r^{(n)} + \mathbf{E}_u \delta_u^{(n)}, \quad (6)$$

where  $\mathbf{D}$  is the average shape velocities of the observed data in the local phase window, and  $(\mathbf{E}_r, \mathbf{E}_u)$  are the terms that describe how shape and input offsets respectively modify the average behavior.  $\delta_r^{(n)} := r^{(n)} - \theta_r^m$ ,  $\delta_u^{(n)} := u^{(n)} - \theta_u^m$  are the shape and input perturbations defined in the  $m^{\text{th}}$  local phase window, where  $(\theta_r^m, \theta_u^m)$  are the mean values of shape and input.

The estimation of the local connection can be done separately from the actuator dynamics, hence this part remains identical as in II-B. We repeat the same procedure for all discrete phase windows and use a Fourier series to smoothly connect all local models.

The fitted models from (6) and (3) can be used in series to make predictions of the system shape and position trajectories given the input signal. First, the input signal  $u(t)$  is transformed into phase coordinate using the fitted phase map. The initial shape is assumed to be on the limit cycle ( $\delta_r = 0$ ) as the same phase value of the initial input  $u(t_0)$ . At each discrete time  $t_i$ , the shape velocity perturbation  $\dot{\delta}_r(t_i)$  is predicted using the actuator model (6) given the current shape perturbation  $\delta_r(t_i)$  and the input perturbation  $\delta_u(t_i)$ .  $\delta_r(t_i)$  is then integrated by Euler method to obtain the predicted shape at the next time step  $\delta_r(t_{i+1})$ . The predicted shape  $\delta_r(t_i)$  is then used to predict the body velocity  $\xi(t_i)$  using the body velocity model (3). The predicted body frame position at the next time step  $g(t_{i+1})$  is then integrated using  $\xi(t_i)$ .

When building an actuator model, the system shape trajectory is the integrated estimation of the shape velocity predictions. Simultaneously, it also appears as the input to the local connection in the locomotion model. As in prior work, the shape and body motion models are predicted in separate stages. Note that in the process of simulating a system spatial trajectory from a general input signal, the two integration steps of each model evolve in series. We start with knowledge of the initial system shape  $r(t=0)$  and the control input  $u(t)$ . Then we can numerically solve (4) and (1) together using the fitted regression models, (6) and (3).

We apply the model improvement metric described in [19], comparing our first order regression model predictions to the phase-averaged baseline model predictions,

$$\Gamma_\chi = 1 - \frac{\sum_{n=1}^{\mathcal{N}} \|\chi_D^{(n)} - \chi^{(n)}\|}{\sum_{n=1}^{\mathcal{N}} \|\chi_T^{(n)} - \chi^{(n)}\|}. \quad (7)$$

This improvement metric is defined by one minus the relative error of the data-driven prediction  $\chi_D$  with respect to the baseline prediction  $\chi_T$  over  $\mathcal{N}$  samples of body velocity and shape velocity  $\chi = \{\xi, \dot{r}\}$ .  $\Gamma_\chi \leq 0$  means the data-driven prediction is no better than the phase-averaged prediction, and  $0 < \Gamma_\chi \leq 1$  means that our model can make better predictions than the baseline model, up to perfect reconstruction of the ground truth at  $\Gamma_\chi = 1$ .

### B. Optimizing behaviors and iterative model refinement

Once an initial model is obtained, we can make predictions on the system position trajectories  $g(t)$  by a general control input  $u(t)$ . Using finite difference, we can estimate the gradient and the Hessian of displacement per cycle with respect to the control parameters around the observed data. We can then utilize the estimated gradient and Hessian to numerically optimize the control parameters for certain behaviors of the system (e.g. maximizing the displacement per cycle).

The expense of data collection<sup>1</sup> incentivizes our focus on sample-efficient optimization schemes. Given an input parameterization, we sparsely sample data in the full range of the input space, and build a rough model. According to this rough model, we numerically optimized the input parameters for certain behavioral objectives. Then we zoom in to the region around the optimized parameter and re-sample points in this local area. The model built with sample points in a smaller region will be more refined and predictions made by the refined model more accurate. We iterate between these two processes—optimization and model refinement—so that in the end it converges to a local optimum in the control space. A global optimum is not guaranteed. In Sections IV and V, we demonstrate the methods using a sample objective where we maximize the displacement per cycle and penalize the cycle time.

## IV. ILLUSTRATIVE EXAMPLE: PURCELL SWIMMER WITH LOW BANDWIDTH ACTUATION

Before demonstrating the method on data, it is helpful to make a proof of concept on a simple analytical model, a three-link Purcell swimmer. We modify the model to include low-bandwidth actuation, inspired by the low-bandwidth actuation of our hydrogel robot:

$$\dot{r}_i = c_i(r_i^s(T) - r_i), \quad c_i > 0, i = 1, 2, \quad (8)$$

where  $r_i$  is the  $i^{\text{th}}$  shape variable (joint positions),  $r_i^s(T)$  denotes each joint's steady state equilibrium given temperature, and  $c_i$  is the converging rate of each joint towards its steady state equilibrium. Specifically, the steady state equilibrium  $r_i^s(T)$  is assigned to be linear function of a one-dimensional input signal, temperature  $T$ . We have a bound on temperature

<sup>1</sup>In practice, a typical temperature cycle for our hydrogel crawler takes approximately 6 hours because of the slow actuation kinetics of the material. The FEA simulation is computationally expensive as well; running a 10-cycle simulation on an well-equipped desktop computer takes about 2 days. Both facts make data collections for such systems expensive, thus data efficiency is crucial.

that puts limits on the swimmer's joint angles. The resulting dynamics can be seen in Fig. 2.

Assuming different constants  $c_i$  on the two joints, the shape variables will exhibit a gait where both joints are not synchronized under a repeating temperature cycle, see Fig. 3. Although both joints are controlled by the same temperature input, the phase lag between the two joints breaks the symmetry of joint synchronization, making the gait enclose a nonzero area in the shape space, which is critical for locomotion in viscous swimming domains from the scallop theorem [31].

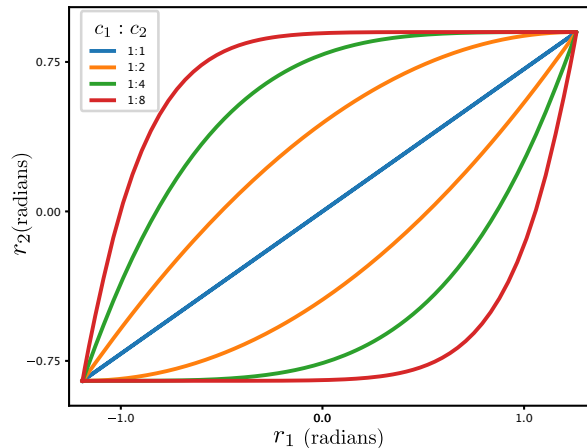


Fig. 2. Plotted on the shape space, phase lag induced shape trajectories exhibit the hysteresis often observed in low bandwidth control systems. The greater the difference in the reaching rate  $c_i$ , the larger the phase lag is. This behavior emerges by waiting for sufficient amount of time for the two joints to both reach steady state equilibrium, and then exciting both joints by a step change in input.

### A. Input generation

Our parameterization on the control signal is concise while maintaining the ability to alter important features of the temperature profile. Here, we used 4 parameters to describe the temperature cycle: a low-point temperature  $T_{\text{low}}$ , a high-point temperature  $T_{\text{high}}$ , time span per cycle  $t_{\text{cycle}}$ , and the portion of the half period to ramp between high and low temperatures  $\eta_{\text{ramp}} = 2t_{\text{ramp}}/t_{\text{cycle}}$ , where  $t_{\text{ramp}}$  is the time to ramp between high and low temperatures, see Fig. 3. Performing multiple cycles of these parameterized temperature cycles, the shape trajectory forms a stable orbit under periodic forcing. We then perturbed the forcing parameters across cycles, which resulted in what can be seen as a "tube" around the orbit as shown in Fig. 5.

## V. MAIN APPLICATION: HYDROGEL CRAWLER

### A. Actuator dynamics

Bilayers and other multi-material structures are useful in creating interesting modes of shape changes like bending. Typical swelling-driven bilayer bending dynamics are similar to the form of an exponential low-pass filter as shown in

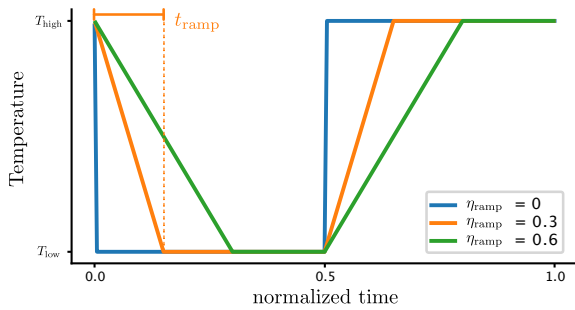


Fig. 3. Example temperature cycles (our low bandwidth control input), normalized for period and temperature, where  $t_{\text{ramp}} = \eta_{\text{ramp}} \cdot t_{\text{cycle}}/2$  is the time used to ramp input to the goal temperature. Since the ramp time should always be smaller than half of the period, the use of ramp time ratio avoids additional constraints other than a bounding box. When  $\eta_{\text{ramp}}$  is small, the temperature profile is more square-wave-like, and the shape trajectory is more likely to have larger phase lag. Consequently, for longer ramp times, the shape trajectory is more likely to have minimal phase lag because both joints are in equilibrium for the duration of temperature change.

Fig. 2. Specifically, the geometry of the bilayer (e.g., layer thickness ratio and material properties) can affect the steady state equilibrium of the shape variables as well as the rate of reaching equilibrium.

### B. Hydrogel crawler

Thermo-responsive hydrogel crawlers in [20], capable of swelling and shrinking, utilize geometric asymmetry, leading to asymmetry in friction forces, to generate net motion under temperature cycles. We utilized the same 2D finite element model in Abaqus Unified FEA [32] to produce time-dependent  $x - y$  coordinate along the contour of the robot to calculate area (2-D volume) of the locomoting segments. The data is then parameterized into the shape variable  $r$ .

Here we assume the actuation dynamics in a general (nonlinear) form (4), without any specific structure on it, namely

$$\dot{r} = f(r, T), \quad (9)$$

where the input is assumed to be the temperature  $T$ .

### C. Finite element model

Briefly, our finite element model, based on chemo-mechanics described in [33], solves coupled diffusion-deformation equations for hydrogel undergoing temperature-driven swelling and shrinking. We used Neo-Hookean and Flory-Huggins potentials to describe the entropic elastic behavior of the polymer network and the mixing of polymer-solvent, respectively. The swelling of pNIPAM caused by the lower critical solution temperature (LCST) was modeled by assuming a sigmoidal function for the temperature dependence of the Flory-Huggins interaction parameter. We also assumed that the diffusivity of the water through pNIPAM also increased sigmoidally with temperature across the LCST, which caused the characteristic time of deswelling to be significantly faster than the characteristic time of swelling. We also considered a combined effect of

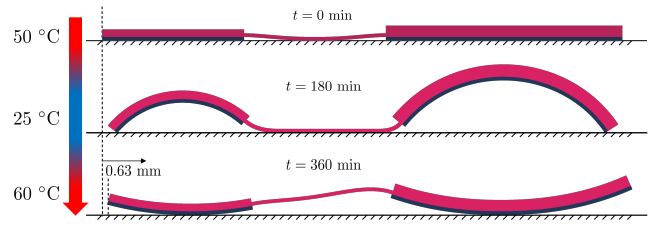


Fig. 4. A representative finite element analysis showing undirectional motion towards the of the larger bilayer of the thermo-responsive hydrogel crawler subjected 3 hours of ramped cooling and 3 hours of ramped heating cycle.

Parameter	Value
Differential density between polymer and water, $\Delta\rho$	100 kg/m <sup>3</sup>
Shear modulus of pNIPAM, $G_{\text{pNIPAM}}$	2.32 kPa
Shear moduli ratio of the gel, $\frac{G_{\text{pAAAM}}}{G_{\text{pNIPAM}}}$	15.36
Curing temperature, $T_{\text{cure}}$	323 K
Flory-Huggins parameter at high temperature, $\chi_H$	0.8031
Flory-Huggins parameter at low temperature, $\chi_L$	1.0483
Transition temperature, $T_{\text{trans}}$	318 K
Range of transition temperature, $\Delta$	8.0
Diffusivity at low temperature, $D_L$	10 <sup>-11</sup> m <sup>2</sup> /s
Diffusivity at high temperature, $D_H$	10 <sup>-10</sup> m <sup>2</sup> /s

TABLE I

LIST OF MATERIALS PROPERTIES USED IN THE SIMULATION

gravity and buoyancy by prescribing a net body force on the hydrogel structure. Our material model included a total of 10 parameters which were either directly determined from experiments or calibrated against experiments using finite element analysis. A list of the parameters and their values are listed in Table V-C. In addition, we assumed a rigid frictional surface with a friction coefficient,  $\mu_k = 0.1$ , underneath the robot to facilitate friction-driven locomotion induced by geometric asymmetry. Further details of the finite element simulation can be found in [20].

### D. Input generation

Here we used a similar parameterization for the input temperature signal as that in IV-A. However, for thermo-responsive hydrogels, the kinetics of the swelling and shrinking vary distinctively. We therefore separated the input cycle into two independent parts, cooling and heating. Thus, the dimension of the input parameter space increases to six, low temperature  $T_{\text{low}}$ , ramped cooling time span  $t_{\text{cool}}$ , cooling ramp time ratio  $\eta_{\text{cool}}$ , high temperature  $T_{\text{high}}$ , ramped heating time span  $t_{\text{heat}}$ , and heating ramp time ratio  $\eta_{\text{heat}}$ . The ramp time ratios are defined as the ratio of the corresponding ramp time to the cooling or heating time span, i.e.,  $\eta_{\text{cool}} = t_{\{\text{ramp,cool}\}}/t_{\text{cool}}$ . The allowable range of each parameter is determined by material properties and characteristic diffusion time and were validated by a parametric study using FEA. Specifically, the ramped cooling and heating time spans are determined by scaling swelling and shrinking characteristic time of the hydrogel, low and high temperature ranges are specified by 4% equilibrium strain span of the material. The ramp ratios are ideally in the range of [0, 1], but small

Parameter	Range
$T_{\text{low}}$	20 $\sim$ 41 $^{\circ}\text{C}$
$T_{\text{high}}$	45 $\sim$ 65 $^{\circ}\text{C}$
$t_{\text{cool}}$	2 $\sim$ 8 hrs
$t_{\text{heat}}$	0.5 $\sim$ 3 hrs
$\eta_{\text{cool}}$	$\frac{1}{32} \sim 1$
$\eta_{\text{heat}}$	$\frac{1}{32} \sim 1$

TABLE II  
FULL INPUT PARAMETER RANGES.

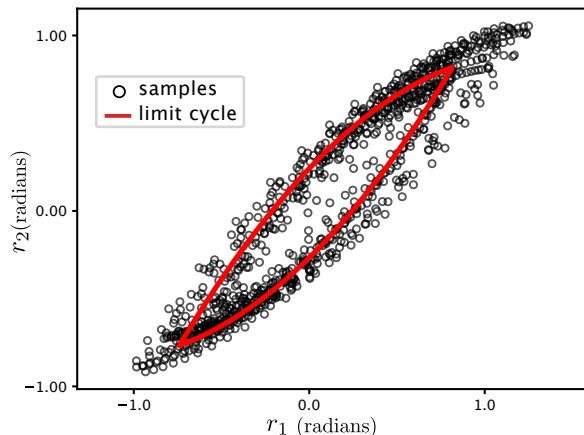


Fig. 5. Sampled shape data points around a limit cycle. Note that we cannot directly sample the full shape and shape velocity space due to the presence of the actuator dynamics. Fortunately, adding perturbation to the input parameters does generate shape and shape velocity variations around the limit cycle, which is essential for building models of behaviors.

ramp ratios means very large rates of temperature change, which is impractical and often causes numerical stability and convergence issues in FEA simulation because of the excessive deformation of the finite element mesh in a short period of time. Thus in the implementations we raised the lower bounds to  $\frac{1}{32}$ . The calculated full input parameter ranges are shown in Table V-D. The noisy input signal is generated by sampling from a uniform distribution in the parameter space. The input parameters are then used to generate noisy temperature cycles for FEA. To avoid numerical issues, instead of running hundreds of thermal cycles at a time, our each FEA simulations comprised of 10 thermal cycles. At each iteration, we ran 10 simulations resulting in 100 cycles of input data for our data-driven model.

### E. Shape parameterization

The soft nature of the devices and external forces makes the shape of the device high dimensional. However, fitting models to a high dimensional shape space will likely cause overfitting. We thus seek a reduced-order representation of the shape of the system. Here, principal components analysis (PCA) is a simple candidate reduction method that could serve this purpose. We tried PCA on the streamline along the crawler body, from which we calculated the internal

angles between each of the segments. Fitting a PCA model on the internal angles, we found that the first two principal components (modes) reconstructs up over 90% of the data. While it is a straight forward way of reducing the effective degrees of freedom, the complex coupling between segments led to principal components that lacked a clear physical interpretation. As an alternative, we considered volume of each active section is a more physical, descriptive candidate for representing the system shape variables. To do this, we estimated the volume at each time point based on contour points from the FEA simulation, and used this to calculate the enclosed area (2D volume for our planar FEA). This parameterization provided a clear, intuitive relationship between the two segments, and exhibited the phase lag between the smaller and larger bilayer segments that we expected from the design.

### F. Input optimization

As a demonstration, we optimized the input parameters to maximize the displacement per cycle. The objective function is defined as

$$F(u) = \Delta g_x - \lambda t_{\text{cycle}}, \quad (10)$$

where  $\Delta g_x$  is the displacement in the  $x$  direction per cycle, and  $t_{\text{cycle}}$  is the cycle time.  $\lambda$  is a penalty factor that controls the trade-off between the above two terms. The objective function is to mainly maximize the net displacement per cycle. During the optimization process, we noticed that the optimizer tended to find cycles with the longest possible cycle times, optimizing cycle-to-cycle distance, with no penalty on time, pushing the results toward the boundary. To address this, we added a regularizing term to penalize the cycle time.

We started by sampling 100 points (resulting 100 cycles of system motion) in the full input parameter space as shown in Table V-D. We performed ten-fold cross validation to avoid overfitting. A rough model of the system was built using the sampled data points, and then the model was used to optimize for an input parameter that maximizes the objective function above. The optimization was performed using the Sequential Least Squares Programming algorithm where the local gradient and Hessian were estimated using finite differencing. After getting the numerical optimum, we shrank each of the input parameter ranges by 35%, centering at the optimum, and repeated the optimization process. We repeat this process three times, and the model improvement metrics were calculated for each iteration as shown in Fig. 6

## VI. DISCUSSION AND CONCLUSION

In this work, we designed and implemented a data-driven modeling framework for dissipative systems with low bandwidth actuator dynamics. We showed the success of this method in predicting behaviors on a classical toy example, the Purcell swimmer, with a modified class of passive shape dynamics. Built on prior work, where at least one shape element is assumed to be accessed through high bandwidth control, this method enables modeling of novel mechanisms like the hydrogel crawler, whose internal

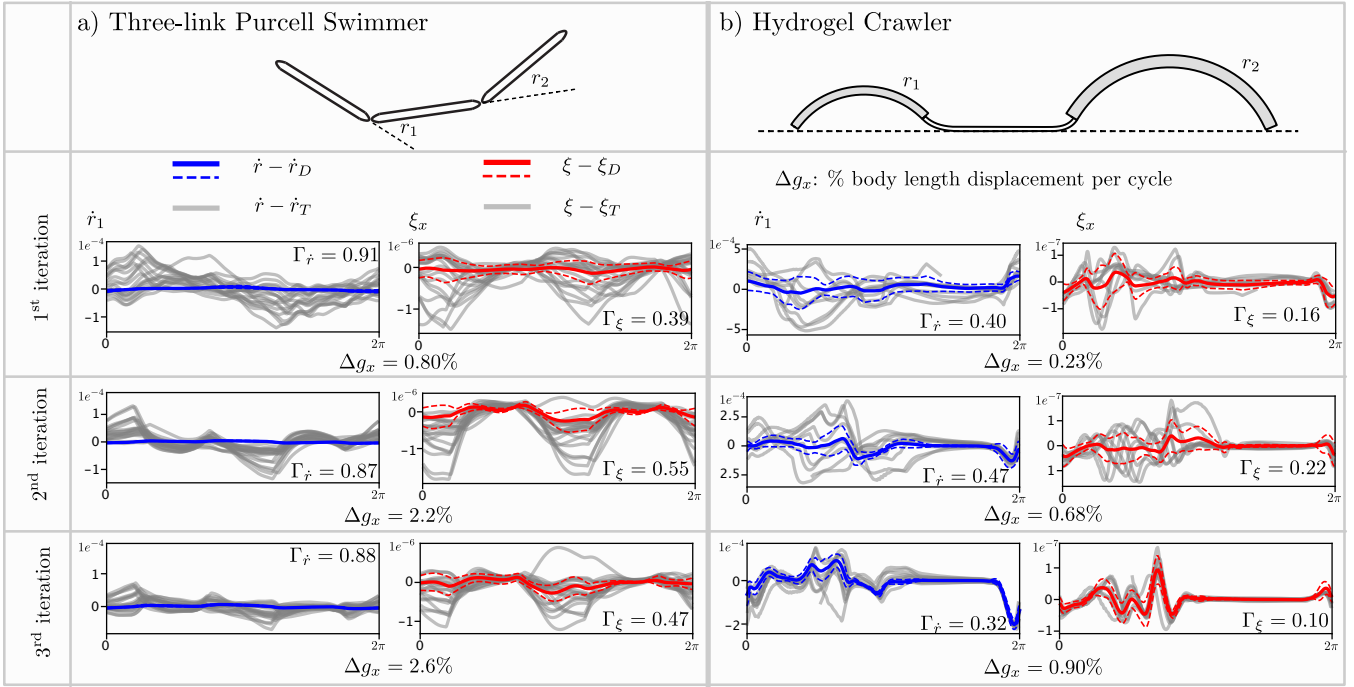


Fig. 6. Model prediction metrics for the Purcell swimmer (top left) and hydrogel crawler (top right) model. We plot sample model prediction errors in phase coordinates from each of the model refining iterations. Also, the average displacement, in terms of percentage body length per actuation cycle, each iteration is shown below the plots. The metrics are calculated on the testing set which is unseen by the model both on shape velocity predictions and body velocity predictions. Test set trajectories (grey) along with the mean (solid) and standard deviation (dashed) of the data-driven model prediction error are plotted for each iteration. The body velocity prediction error is inherently propagated from the shape velocity prediction error, and thus the body velocity prediction errors are unsurprisingly greater than the shape velocity prediction error. While the model prediction errors starts to drop as we shrink the sampling range due to overfitting, the average behavioral objective is improving each iteration.

degrees of freedom all exhibit a passive response to controllable stimuli. We showed not only that we could model the crawler with accuracy beyond the phase averaged gait, but that the system was capable of using this model in a gradient-based optimization scheme to rapidly identify a viable crawling maneuver. The broader implications of this result are that we now have a justifiable framework to pursue data-driven modeling and optimization of a much larger class of underactuated systems. For applications in biology, where continuous, soft interfaces facilitate safe interaction with the body, this method provides the potential to model new mechanisms pre-deployment in the body and even *in situ*, since variation amongst morphology and environment across patients can be significant. Key additional efforts for such endeavors require power, actuation, and sensing at the scales desired for the locomotion application.

Implementing our motivated prediction architecture on the Purcell swimmer provided insight in to what prediction quality was achievable on a toy system. The models have significant prediction improvement with respect to the phase-averaged model. This provides a level of accuracy in predicting the neighborhood of behaviors about that gait, suggesting that a gradient-based optimization may work reliably. On the hydrogel crawler, we observe improved prediction quality with respect to the phase model. While this prediction quality is lower than what was observed in the toy example, it is enough insight to successfully inform a gradient-based

optimization scheme.

While it is not possible for us to assert global optimality, we have shown that the model was iteratively improved and appeared to settle at a performant lunging gait. Sampling from a variety of initial conditions could excite a variety of achieved locally optimal gaits, from which a more globally optimal gait could be selected. If the hydrogels objective were simply to obtain a functional navigation policy, we have provided a framework through which it and similar robots can rapidly obtain functional motion primitives.

The model improvement saturated and decayed as the sampling region was reduced, likely because there were few variations in the sampled data. It is well known that the convergence properties proved in adaptive control rely on sufficient excitation of the dynamics, and likewise, we don't expect to learn informative improvement without cycles that excite significant dynamic variation. We have learned to be careful in reducing the sampling region as it may cause the data-driven model to degrade.

The viable gaits achieved through this sample efficient optimization could practically extend to the real world. While many samples might be available in simulated environments, there are many platforms that must be system-identified in the field. *In-situ* system identification (such as the type we implement here) paired with a gradient-based optimizer provides a tractable, systems oriented way to pursue optimization of robot behaviors in hard-to-model environments.

The sample-efficiency was even highly valuable for this project, where a single cycle takes several hours to simulate.

## REFERENCES

- [1] D. Trivedi, C. D. Rahn, W. M. Kier, and I. D. Walker, "Soft robotics: Biological inspiration, state of the art, and future research," *Applied Bionics and Biomechanics*, vol. 5, pp. 99–117, 2008.
- [2] R. F. Shepherd, F. Ilievski, W. Choi, S. A. Morin, A. A. Stokes, A. D. Mazzeo, X. Chen, M. Wang, and G. M. Whitesides, "Multigait soft robot," *Proceedings of the National Academy of Sciences*, vol. 108, no. 51, pp. 20400–20403, 2011.
- [3] B. Liu, Y. Ozkan-Aydin, D. I. Goldman, and F. L. Hammond, "Kirigami skin improves soft earthworm robot anchoring and locomotion under cohesive soil," in *2019 2nd IEEE International Conference on Soft Robotics (RoboSoft)*. IEEE, 2019, pp. 828–833.
- [4] Y. O. Aydin, J. L. Molnar, D. I. Goldman, and F. L. Hammond, "Design of a soft robophysical earthworm model," in *2018 IEEE International Conference on Soft Robotics (RoboSoft)*. IEEE, 2018, pp. 83–87.
- [5] H. Zhao, Y. Li, A. Elsamadisi, and R. Shepherd, "Scalable manufacturing of high force wearable soft actuators," *Extreme Mechanics Letters*, vol. 3, pp. 89–104, 2015.
- [6] H. Lu, M. Zhang, Y. Yang, Q. Huang, T. Fukuda, Z. Wang, and Y. Shen, "A bioinspired multilegged soft millirobot that functions in both dry and wet conditions," *Nature Communications*, vol. 9, no. 1, p. 3944, 2018.
- [7] T. TolleyMichael, F. ShepherdRobert, C. GallowayKevin, J. WoodRobert, M. WhitesidesGeorge, et al., "A resilient, untethered soft robot," *Soft Robotics*, 2014.
- [8] S. I. Rich, R. J. Wood, and C. Majidi, "Untethered soft robotics," *Nature Electronics*, vol. 1, no. 2, pp. 102–112, 2018.
- [9] M. Li, X. Wang, B. Dong, and M. Sitti, "In-air fast response and high speed jumping and rolling of a light-driven hydrogel actuator," *Nature Communications*, vol. 11, no. 1, p. 3988, 2020.
- [10] C. Li, G. C. Lau, H. Yuan, A. Aggarwal, V. L. Dominguez, S. Liu, H. Sai, L. C. Palmer, N. A. Sather, T. J. Pearson, et al., "Fast and programmable locomotion of hydrogel-metal hybrids under light and magnetic fields," *Science Robotics*, vol. 5, no. 49, p. eabb9822, 2020.
- [11] S. Wu, Q. Ze, R. Zhang, N. Hu, Y. Cheng, F. Yang, and R. Zhao, "Symmetry-breaking actuation mechanism for soft robotics and active metamaterials," *ACS Applied Materials & Interfaces*, vol. 11, no. 44, pp. 41 649–41 658, 2019.
- [12] Q. L. Zhu, C. Du, Y. Dai, M. Daab, M. Matejdes, J. Breu, W. Hong, Q. Zheng, and Z. L. Wu, "Light-steered locomotion of muscle-like hydrogel by self-coordinated shape change and friction modulation," *Nature Communications*, vol. 11, no. 1, p. 5166, 2020.
- [13] R. L. Hatton and H. Choset, "Nonconservativity and noncommutativity in locomotion," *The European Physical Journal Special Topics*, vol. 224, no. 17, pp. 3141–3174, 2015.
- [14] R. L. Hatton, T. Dear, and H. Choset, "Kinematic cartography and the efficiency of viscous swimming," *IEEE Transactions on Robotics*, vol. 33, no. 3, pp. 523–535, 2017.
- [15] Y. Ozkan Aydin, B. Chong, C. Gong, J. M. Rieser, J. W. Rankin, K. Michel, A. G. Nieceza, J. Hutchinson, H. Choset, and D. I. Goldman, "Geometric mechanics applied to tetrapod locomotion on granular media," in *Biomimetic and Biohybrid Systems: 6th International Conference, Living Machines 2017, Stanford, CA, USA, July 26–28, 2017, Proceedings 6*. Springer, 2017, pp. 595–603.
- [16] D. Zhao, B. Bittner, G. Clifton, N. Gravish, and S. Revzen, "Walking is like slithering: A unifying, data-driven view of locomotion," *Proceedings of the National Academy of Sciences*, vol. 119, no. 37, p. e2113222119, 2022.
- [17] S. D. Kelly and R. M. Murray, "Geometric phases and robotic locomotion," *Journal of Robotic Systems*, vol. 12, no. 6, pp. 417–431, 1995.
- [18] B. Bittner, R. L. Hatton, and S. Revzen, "Geometrically optimal gaits: a data-driven approach," *Nonlinear Dynamics*, vol. 94, no. 3, pp. 1933–1948, 2018.
- [19] —, "Data-driven geometric system identification for shape-underactuated dissipative systems," *Bioinspiration & Biomimetics*, vol. 17, no. 2, p. 026004, jan 2022.
- [20] A. Pantula, B. Datta, Y. Shi, M. Wang, J. Liu, S. Deng, N. J. Cowan, T. D. Nguyen, and D. H. Gracias, "Untethered unidirectionally crawling gels driven by asymmetry in contact forces," *Science Robotics*, vol. 7, no. 73, p. eadd2903, 2022.
- [21] J. C. Breger, C. Yoon, R. Xiao, H. R. Kwag, M. O. Wang, J. P. Fisher, T. D. Nguyen, and D. H. Gracias, "Self-folding thermo-magnetically responsive soft microgrippers," *ACS applied materials & interfaces*, vol. 7, no. 5, pp. 3398–3405, 2015.
- [22] D. Han, C. Farino, C. Yang, T. Scott, D. Browe, W. Choi, J. W. Freeman, and H. Lee, "Soft robotic manipulation and locomotion with a 3d printed electroactive hydrogel," *ACS applied materials & interfaces*, vol. 10, no. 21, pp. 17 512–17 518, 2018.
- [23] H. Na, Y.-W. Kang, C. S. Park, S. Jung, H.-Y. Kim, and J.-Y. Sun, "Hydrogel-based strong and fast actuators by electroosmotic turgor pressure," *Science*, vol. 376, no. 6590, pp. 301–307, 2022.
- [24] H. Cendra, J. E. Marsden, and T. S. Ratiu, "Geometric mechanics, lagrangian reduction, and nonholonomic systems," *Mathematics Unlimited—2001 and Beyond*, pp. 221–273, 2001.
- [25] A. M. Bloch, *Nonholonomic Mechanics and Control*. Springer New York, NY, 2003.
- [26] J. P. Ostrowski, J. P. Desai, and V. Kumar, "Optimal gait selection for nonholonomic locomotion systems," *The International Journal of Robotics Research*, vol. 19, no. 3, pp. 225–237, 2000.
- [27] S. D. Kelly and R. M. Murray, "The geometry and control of dissipative systems," in *Proceedings of 35th IEEE Conference on Decision and Control*, vol. 1. IEEE, 1996, pp. 981–986.
- [28] J. Dai, H. Faraji, C. Gong, R. L. Hatton, D. I. Goldman, and H. Choset, "Geometric swimming on a granular surface," in *Robotics: Science and Systems*, 2016.
- [29] S. Revzen and J. M. Guckenheimer, "Estimating the phase of synchronized oscillators," *Physical Review E*, vol. 78, p. 051907, Nov 2008.
- [30] S. Revzen and M. Kvalheim, "Data driven models of legged locomotion," in *Micro- and Nanotechnology Sensors, Systems, and Applications VII*, T. George, A. K. Dutta, and M. S. Islam, Eds., vol. 9467, International Society for Optics and Photonics. SPIE, 2015, p. 94671V.
- [31] E. M. Purcell, "Life at low reynolds number," *American journal of physics*, vol. 45, no. 1, pp. 3–11, 1977.
- [32] "Abaqus/standard, version 2021," United States, 2021.
- [33] S. A. Chester and L. Anand, "A thermo-mechanically coupled theory for fluid permeation in elastomeric materials: Application to thermally responsive gels," *Journal of the Mechanics and Physics of Solids*, vol. 59, no. 10, pp. 1978–2006, 2011. [Online]. Available: <https://www.sciencedirect.com/science/article/pii/S0022509611001426>